

01,14

Optimization of physical and mechanical properties of ultrafine-grained Al-Mg-Zr alloy for electrical purposes

© T.S. Orlova, D.I. Sadykov, D.A. Kirilenko, A.I. Likhachev, A.A. Levin

Ioffe Institute, Russian Academy of Sciences,
St. Petersburg, Russia

E-mail: orlova.t@mail.ioffe.ru

Received March 3, 2025

Revised March 12, 2025

Accepted March 13, 2025

For the ultrafine-grained (UFG) Al-0.95Mg-0.32Zr (wt.%), alloy structured by high-pressure torsion (HPT), a unique combination of strength (390 MPa), ductility ($\sim 10\%$) and electrical conductivity ($\sim 49\%$ IACS — International Annealed Copper Standard) was achieved due to additional deformation-heat treatment (DHT), consisting of annealing at an elevated temperature of 230°C for 1 h and a small additional deformation by HPT. The evolution of microstructure at both stages of DHT was studied. The analysis of the microstructure-property relationship showed that the achieved ductility is provided by the introduction of an additional dislocation density into the anneal-relaxed grain boundary (GB) structure and near-boundary regions as a result of DHT, as well as the formation of a significant fraction ($\sim 20\%$) of larger grains with a size of ≥ 900 nm in the UFG structure. The retention of strength after DHT at a level of $\sim 75\%$ of the strength in the initial UFG state can be explained by the retention of a small average grain size (510 nm) and the formation of new Mg segregations at GBs.

Keywords: aluminum alloys, ultrafine-grained structure, strength, ductility, grain boundaries, segregation, dislocations.

DOI: 10.61011/PSS.2025.03.60870.49-25

1. Introduction

Ultrafine-grained (UFG) low-alloyed aluminum alloys structured by methods of severe plastic deformation (SPD) are seen as promising candidates for conductor materials of the new generation [1,2]. The alloying additives used firstly include Zr in the concentrations of up to 0.6 wt.%, since when annealed at temperatures $350\text{--}450^\circ\text{C}$ Zr may form the nanoscale inclusions of the secondary phase Al_3Zr , contributing to the stabilization of strength properties at higher temperatures [3–7]. However, alloying with Zr alone will not provide the strength high enough in the alloys of the Al–Zr system even in the UFG state, therefore this system is additionally alloyed. Mg is a suitable alloying element, since it promotes efficient grain refinement in process of structuring by the SPD methods [8,9]. Previously it was shown that a small addition of Mg (0.5–1.2 wt.%) to the Al–Zr system causes significant strengthening after structuring by high-pressure torsion (HPT) method [10] and equal channel angular pressing (ECAP) [11]. However, the ductility at the same time drops below the level necessary for the practical application.

To improve the ductility of UFG alloys Al-(0.5–1.2)Mg-(0.27–0.34)Zr (wt.%) with strength maintenance at a high level, we previously offered an approach consisting of low-temperature annealing and a small additional deformation (AD) by HPT to 0.25 turns [12,13]. It was shown that such deformation-heat treatment (DHT) leads to relaxation of the grain boundaries when annealed without significant change in the grain size

and to introduction of additional extrinsic dislocations by the additional deformation into the relaxed structure of the grain boundaries (GB), which helped to significantly improve ductility [12,13]. At the same time even though the strength decreases, it remains at a relatively high level (at the level of $\sim 80\%$ of the strength of initial UFG state prior to DHT). It should be noted that as the concentration of the alloying element Mg increases from 0.5 to 1.2 wt.%, the ductility value achieved by this DHT (annealing + AD) δ decreases [13]. For example, in the alloy Al-1.17Mg-0.32Zr (wt.%) it only amounted to $\delta \approx 5\%$ (elongation to failure).

This paper proposes an alternative approach to optimize the properties of strength-ductility-electrical conductivity of low-alloyed UFG-alloys of Al-Mg-Zr system using the example of alloy Al-0.95Mg-0.32Zr (wt.%), causing a more significant increase of ductility at the expense of only a small decrease in the strength while maintaining the level of electrical conductivity. In the proposed approach, the annealing is used at elevated temperature, and some additional deformation by HPT, which made it possible to both change the dislocation structure of GBs and change the distribution of grains on size, which provided for optimization of the properties: strength–ductility.

2. Specimens and experimental methods

The experimental ternary alloy Al-0.95Mg-0.32Zr (wt.%) was studied. The original bars of the alloy were produced by

casting method with subsequent hot rolling at $T = 300^\circ\text{C}$ in the National Research Technology University „MISIS“ (Moscow, Russia) and are specified in more detail in [14]. The selected rolling temperature ensures minimum uncontrolled decomposition of the solid solution of aluminum supersaturated with zirconium, which is formed during the alloy crystallization [10].

To homogenize the solid solution and deposit the nanoscale precipitates (NPs) of meta-stable phase Al_3Zr (L_{12}) [3–7], the alloy bars with diameter $d = 12\text{ mm}$ were exposed to artificial aging (aging — AG) at temperature of 375°C for 140 h. The UFG structure of the original coarse-grained (CG) specimens was formed by the HPT method at pressure $P = 2\text{ GPa}$ and number of turns $n = 10$ under the room temperature (RT) conditions. For treatment by HPT method, the cylindrical billets with a diameter of $d = 12\text{ mm}$ and a height of $h = 4.2\text{ mm}$ were used, which after the HPT-processing acquired the shape of discs with $d = 20\text{ mm}$ and $h = 1.2\text{ mm}$. This state is hereinafter referred to as HPT. Some UFG-specimens in the form of discs were exposed to additional annealing at $T_{\text{AN}} = 230^\circ\text{C}$ for 1 h (state HPT + AN(230)) with and without subsequent additional deformation by HPT method to $n = 0.25$ turns under $P = 2\text{ GPa}$ at RT (state HPT + AN(230) + 0.25HPT). Such deformation-heat treatment of „annealing at elevated temperature (AET) + AD“ type is further indicated as DHT.

The microstructure of the alloy Al-0.95Mg-0.32Zr (wt.%) in different states was studied by different complementary methods, such as transmission electron microscopy and scanning transmission electron microscopy (TEM/STEM), X-ray diffraction analysis (XDA), electron backscatter diffraction (EBSD) and energy-dispersive X-ray spectroscopy (EDXS).

The studies using TEM and STEM methods were carried out on a JEOL JEM-2100F microscope under accelerating voltage of 200 kV and resolution of 0.19 nm/dot, the EDXS studies were carried out *in situ* in STEM with probe $\leq 1\text{ nm}$. Foils for electron microscopy studies were made by mechanical polishing and subsequent double-jet electrochemical polishing in the solution of nitric acid (20%) and ethanol (80%) at temperature of -10°C and operating voltage of 18 V.

XDA was carried out using powder X-ray diffractometer D2 Phaser (Bruker AXS, Germany) with Bragg–Brentano vertical geometry and $\text{CuK}\alpha$ -emission (average wavelength $\lambda = 1.5418\text{ \AA}$), filtered by nickel foil. To detect an X-ray diffraction (XRD) signal, semiconductor linear position-sensitive detector LYNXEYE (Bruker AXS) was used. X-ray measurements were carried out in the mode of symmetrical θ – 2θ scanning. X-ray diffraction analysis of the measured diffraction patterns was performed using the EVA software [15] in the combination with the Powder Diffraction File-2 (PDF-2) [16] database.

The cubic unit cell parameter a of aluminum alloy in the studied states was calculated using Bragg angles $2\theta_{hkl}$ of all observed X-ray reflexes of Al, adjusted with angular

corrections, and their Miller indices hkl by the least-square method using Celsiz software [17].

The calculation of the average size of coherent scattering domains (D_{CSD}) and average absolute value of microstrain ε_s (also known as a level of elastic microdistortions $\langle\varepsilon^2\rangle^{1/2}$) was done in SizeCr software [18] using the values of full widths of reflexes at half maximum (FWHM) by two different graphic methods: Williamson–Hall plot (WHP) building method [19] and „crystallite size — microstrain plot“ (size-strain plot, SSP) building method [20]. The procedures were used to adjust the instrumental input to FWHM and to calculate the WHP and SSP for the reflections with the profiles described by Vogt pseudo-function [18–20], which were observed in measured XRD patterns.

The value of integral density of dislocations (L_{dis}) was determined using formula [21,22]

$$L_{\text{dis}} = \frac{2\sqrt{3}\langle\varepsilon^2\rangle^{1/2}}{D_{\text{CSD}} \cdot b}, \quad (1)$$

where b — value of Burgers vector of lattice dislocation in Al (0.286 nm [23]).

To do the studies using the EBSD method, scanning electron microscope (SEM) JSM 7001F (JEOL, Japan), equipped with detector HKL Nordlys EBSD Detector (Oxford Instruments, England) was used. The specimen surface was radiated by an electron beam with energy of 10 keV at angle 70° to the normal line to the specimen surface. The size of the scanning area was $20 \times 20\text{ }\mu\text{m}^2$, scanning step was 50 nm. The resulting EBSD maps included minimum 1000 grains for each state and were used to determine the average grain size (d_G), the fraction of high-angle boundaries ($f_{\geq 15}$), and the average misorientation angle (θ_{av}). The grain size in the EBSD method was calculated as the diameter of circumference with the area equivalent to the grain size. The grain boundaries with misorientation $2.0 < \theta < 15^\circ$ were referred to low-angle grain boundaries (LAGBs), and with misorientation $\theta \geq 15^\circ$ to high-angle grain boundaries (HAGBs).

The mechanical properties were studied by tensile tests on a Shimadzu AG-50kNX testing machine at constant strain rate $\dot{\varepsilon} = 5 \cdot 10^{-4}\text{ s}^{-1}$. For tensile tests, specimens were used in the form of flat blades with working part size of $2 \times 1 \times 6\text{ mm}^3$, cut from the discs at the distance of 5 mm from the disc center. The tests were done at RT. The specimens deformations were measured using a video extensometer TRViewX 55S. According to the results of mechanical tests, the values of yield stress ($\sigma_{0.2}$), ultimate tensile strength (σ_{UTS}) and elongation to failure (δ), and also uniform elongation (δ_1) were determined. To obtain the valid results, minimum three specimens were tested for every state.

Electrical conductivity was determined in accordance with the requirements of GOST 27333–87 „Nondestructive testing. Measurement of electrical conductivity of non-ferrous metals by eddy current method“ using eddy current

Table 1. Physical and mechanical properties of UFG-alloy Al-0.95Mg-0.32Zr (wt.%) in various states

State	$\sigma_{0.2}$, MPa	σ_{UTS} , MPa	δ , %	δ_1 , %	ω , MS/m	ω , % IACS	Reference
HPT	440 ± 15	557 ± 10*	1.4 ± 0.4	–	27.6 ± 0.2	47.5 ± 0.4	Pres. paper
HPT + AN(230)	211 ± 5	219 ± 6	12.6 ± 1.4	0.4 ± 0.1	29.0 ± 0.2	50.1 ± 0.3	
HPT + AN(230) + 0.25HPT	336 ± 5	389 ± 8	10 ± 1.2	2.4 ± 0.2	28.1 ± 0.2	48.4 ± 0.3	
HPT + AN(150)	371 ± 8	414 ± 6*	0.6 ± 0.1	–	28.6 ± 0.2	49.4 ± 0.3	[14]
HPT + AN(150) + 0.25HPT	371 ± 14	458 ± 18	6.9 ± 1.3	2.6 ± 0.5	27.8 ± 0.3	47.9 ± 0.5	

Note. * The values correspond to the fracture stress (σ_R).

meter for non-ferrous metals VE-27NC/4-5 with relative error $\pm 2\%$. The obtained values of electrical conductivity were converted to the international standard units % IACS (International Annealed Copper Standard), using formula

$$\% \text{ IACS} = \frac{\omega_{\text{Al}_{\text{alloy}}}}{\omega_{\text{Cu}}} \cdot 100, \quad (2)$$

where $\omega_{\text{Al}_{\text{alloy}}}$ is electrical conductivity value of the studied Al alloy, ω_{Cu} is electrical conductivity value of copper (58.0 MS/m).

Electrical conductivity measurements, as well as the microstructure studies, were conducted at the distance of 5 mm from the HPT disc center, i.e. in the area in the middle of the work zone of the specimens for mechanical tests cut from discs.

3. Experimental results

3.1. Mechanical properties and electrical conductivity

Figure 1 presents stress–strain curves obtained for UFG-alloy Al-0.95Mg-0.32Zr (wt.%) in different states: HPT, HPT + AN(230) and HPT + AN(230) + 0.25HPT. For comparison, stress–strain curves are provided, which we obtained previously for this alloy in states HPT + AN(150) and HPT + AN(150) + 0.25HPT [14]. The main mechanical characteristics ($\sigma_{0.2}$, σ_{UTS} , δ , δ_1), determined by analysis of the obtained stress–strain curves, and the values of electrical conductivity are given in Table 1.

After HPT structuring the alloy demonstrates high strength ($\sigma_{0.2} \approx 440$ MPa, $\sigma_{UTS} \approx 560$ MPa) and very low ductility $\delta \approx 1.4\%$. Annealing at $T_{AN} = 230^\circ\text{C}$, $t = 1$ h (state HPT + AN(230)) causes sharp decrease in strength at significant increase of ductility (Table 1, Figure 1); the value of $\sigma_{0.2}$ decreased by more than 2 times (from 440 to ~ 210 MPa) with an increase in ductility by almost an order of magnitude (from 1.4 to $\sim 13\%$). Such trend of mechanical characteristics change — decrease of strength at higher ductility because of annealing is specific for CG materials. Additional HPT deformation to $n = 0.25$ turns (state HPT + AN(230) + 0.25HPT) caused significant strength increase: $\sigma_{0.2}$ increased by $\sim 60\%$ (from ~ 210 to ~ 340 MPa), and σ_{UTS} — by $\sim 80\%$ (from 220 to ~ 390 MPa) at minor decrease of ductility

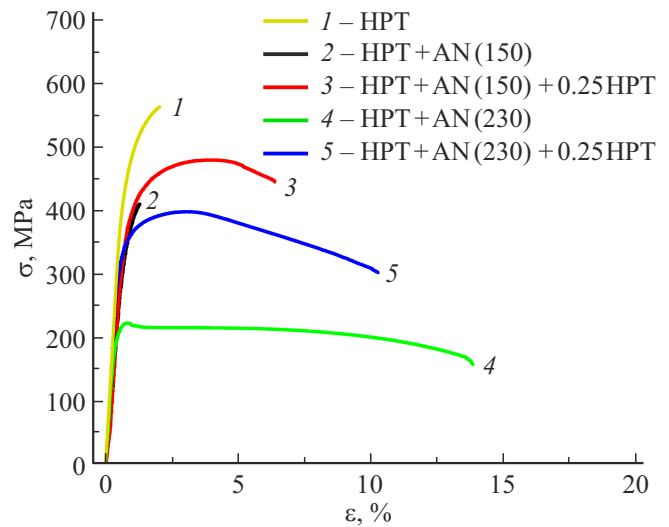


Figure 1. Stress–strain curves obtained from tensile tests of specimens of UFG-alloy Al-0.95Mg-0.32Zr (wt.%) in different states.

from 12.6 to $\sim 10\%$. Such nature of change to mechanical properties — decrease of ductility with increase of strength as a result of additional deformation is also specific for strain-hardened CG alloys. Similarly to the case of annealing at 150°C and AD by HPT to $n = 0.25$ [14], annealing at 230°C and subsequent AD insignificantly change the electrical conductivity: in state HPT $\omega = 47.5\%$ IACS, and in state HPT + AN(230) + 0.25HPT $\omega = 48.4\%$ IACS. This indicates that DHT with $T_{AN} = 230^\circ\text{C}$ (state HPT + AN(230) + 0.25HPT), as well as DHT with $T_{AN} = 150^\circ\text{C}$ (state HPT + AN(150) + 0.25HPT) do not change significantly the concentration of impurity elements in the solid solution.

Therefore, the change of the mechanical properties after DHT with $T_{AN} = 230^\circ\text{C}$ differs essentially from the DHT case with $T_{AN} = 150^\circ\text{C}$, when the annealing decreased the ductility to the brittle state, and subsequent AD caused considerable increase of ductility (deformation-induced softening effect). However, as a result of using DHT with $T_{AN} = 230^\circ\text{C}$ (state HPT + AN(230) + 0.25HPT) a good combination of properties was also achieved: yield stress ~ 340 MPa, ultimate tensile strength ~ 390 MPa, ductility $\delta \approx 10\%$ ($\delta_1 > 2\%$) and electrical conductivity

Table 2. Results of profile analysis of XRD reflexes obtained for UFG-alloy Al-0.95Mg-0.32Zr (wt.%) in different states

State	a , Å	WHP			SSP			Reference
		D_{CSD} , nm	ε_s , %	L_{dis} , 10^{13} m^{-2}	D_{CSD} , nm	ε_s , %	L_{dis} , 10^{13} m^{-2}	
HPT	4.0530 ± 0.0004	128 ± 21	0.066 ± 0.004	6.2 ± 1.1	119 ± 9	0.064 ± 0.003	6.5 ± 0.6	Pres. paper
HPT + AN(230)	4.0546 ± 0.0001	218 ± 10	0.014 ± 0.001	0.78 ± 0.1	216 ± 4	0.0142 ± 0.0009	0.80 ± 0.05	
HPT + AN(230) + 0.25HPT	4.0544 ± 0.0001	164 ± 35	0.072 ± 0.004	5.3 ± 1.7	162 ± 22	0.072 ± 0.004	5.4 ± 0.8	
HPT + AN(150)	4.0544 ± 0.0002	181 ± 8	0.018 ± 0.001	1.20 ± 0.09	181 ± 4	0.018 ± 0.001	1.20 ± 0.07	[14]
HPT + AN(150) + 0.25HPT	4.0536 ± 0.0002	130 ± 22	0.067 ± 0.005	6.2 ± 1.2	124 ± 11	0.066 ± 0.004	6.4 ± 1.2	

(48.4% IACS), which is only slightly inferior in strength, but in ductility it significantly exceeds the achieved value δ as a result of using such DHT with $T_{\text{AN}} = 150^\circ\text{C}$ (state HPT + AN(150) + 0.25HPT).

3.2. Evolution of microstructure in process of DHT

To identify the key parameters of the microstructure, which provided the achieved physical and mechanical properties as a result of applying DHT that consists of annealing (230°C , 1 h) and AD (HPT to $n = 0.25$ turns), the microstructural features of the alloy in HPT, HPT + AN(230) and HPT + AN(230) + 0.25HPT states were studied.

Detailed study of the alloy microstructure in HPT state was conducted by us previously [14]. Table 2 presents the results of the profile analysis of the observed XRD reflexes for all studied states.

Both methods (WHP and SSP) for determination of parameters D_{CSD} and ε_s gave close results, and accordingly the close values of the dislocation density (Table 2). Since the standard deviations of the assessed parameters were lower in the case of SSP, further only the values obtained using SSP will be considered.

After annealing $T_{\text{AN}} = 230^\circ\text{C}$ (state HPT + AN(230)), value D_{CSD} increases to 216 nm, value ε_s decreases from 0.064 to $\sim 0.014\%$, which may be explained by the processes of recovery of defect structure during annealing. The subsequent additional deformation (state HPT + AN(230) + 0.25HPT) causes decrease of D_{CSD} to 162 nm and increase of the level of elastic microdistortions ε_s to 0.072%, i.e. the level of elastic microdistortions returns approximately to the level prior to annealing (Table 2). Qualitatively similar effects of increase D_{CSD} to 181 nm and relaxation ε_s to 0.018% are also observed after annealing at $T_{\text{AN}} = 150^\circ\text{C}$ (state HPT + AN(150)). In contrast to the specimen annealed at higher temperature $T_{\text{AN}} = 230^\circ\text{C}$, the specimen after annealing at $T_{\text{AN}} = 150^\circ\text{C}$ and subsequent AD (state HPT + AN(150) + 0.25HPT) returns approximately to the original values by D_{CSD} and ε_s (Table 2).

In the HPT state the density of dislocations was $L_{\text{dis}} = 6.5 \cdot 10^{13} \text{ m}^{-2}$. Annealing at 230°C (state

HPT + AN(230)) caused a more significant decrease in the density of dislocations compared to annealing at 150°C (Table 2). Value L_{dis} dropped approximately ~ 8 times ($L_{\text{dis}} = 0.80 \cdot 10^{13} \text{ m}^{-2}$) after annealing at 230°C and ~ 5 times after annealing at 150°C ($L_{\text{dis}} = 1.2 \cdot 10^{13} \text{ m}^{-2}$), which is related to more effective processes of defect structure recovery and annihilation of dislocations in the process of annealing at higher T_{AN} . Additional deformation to $n = 0.25$ turns causes increase in density of dislocations, returning value L_{dis} practically to the original one in the state prior to annealing (HPT state). In state HPT + AN(150) + 0.25HPT the dislocation density L_{dis} was $6.4 \cdot 10^{13} \text{ m}^{-2}$, and in state HPT + AN(230) + 0.25HPT $L_{\text{dis}} = 5.4 \cdot 10^{13} \text{ m}^{-2}$. The trend towards changing the parameters of the microstructure determined by the profile analysis of XRD patterns, and dislocation density assessed using them at both stages of DHT with $T_{\text{AN}} = 230^\circ\text{C}$ is similar to that in case of DHT with $T_{\text{AN}} = 150^\circ\text{C}$, taking into account the adjustment to the higher annealing temperature. Similar character of changes in the dislocation density as a result of annealing and subsequent small HPT deformation was observed by us previously in UFG alloys Al-1.47Cu-0.34Zr (wt.%) [24] and Al-0.53Mg-0.27Zr (wt.%) [11], also structured by HPT method.

Figure 2 shows typical EBSD-maps and grain distribution on size and GB distribution on the misorientation angles obtained for UFG-Al-0.95Mg-0.32Zr (wt.%) in the following states: HPT, HPT + AN(230) and HPT + AN(230) + 0.25HPT. Main microstructural parameters (average grain size d_G , fraction of high-angle grain boundaries $f_{\geq 15}$, average misorientation angle of grain boundaries θ_{av}) are given in Table 3.

In all the studied states a UFG-structure is observed with the grain shape similar to the equiaxial one, and preferably high-angle misorientation of GB ($f_{\geq 15} > 60\%$) with average grain boundary misorientation angle close to 30° .

In the HPT state the character of grain distribution on size is unimodal, the average grain size is $d_G \sim 410 \text{ nm}$ (Figure 2, a and b). Annealing at 230°C causes increase in the average grain size to $\sim 690 \text{ nm}$; and at the same time

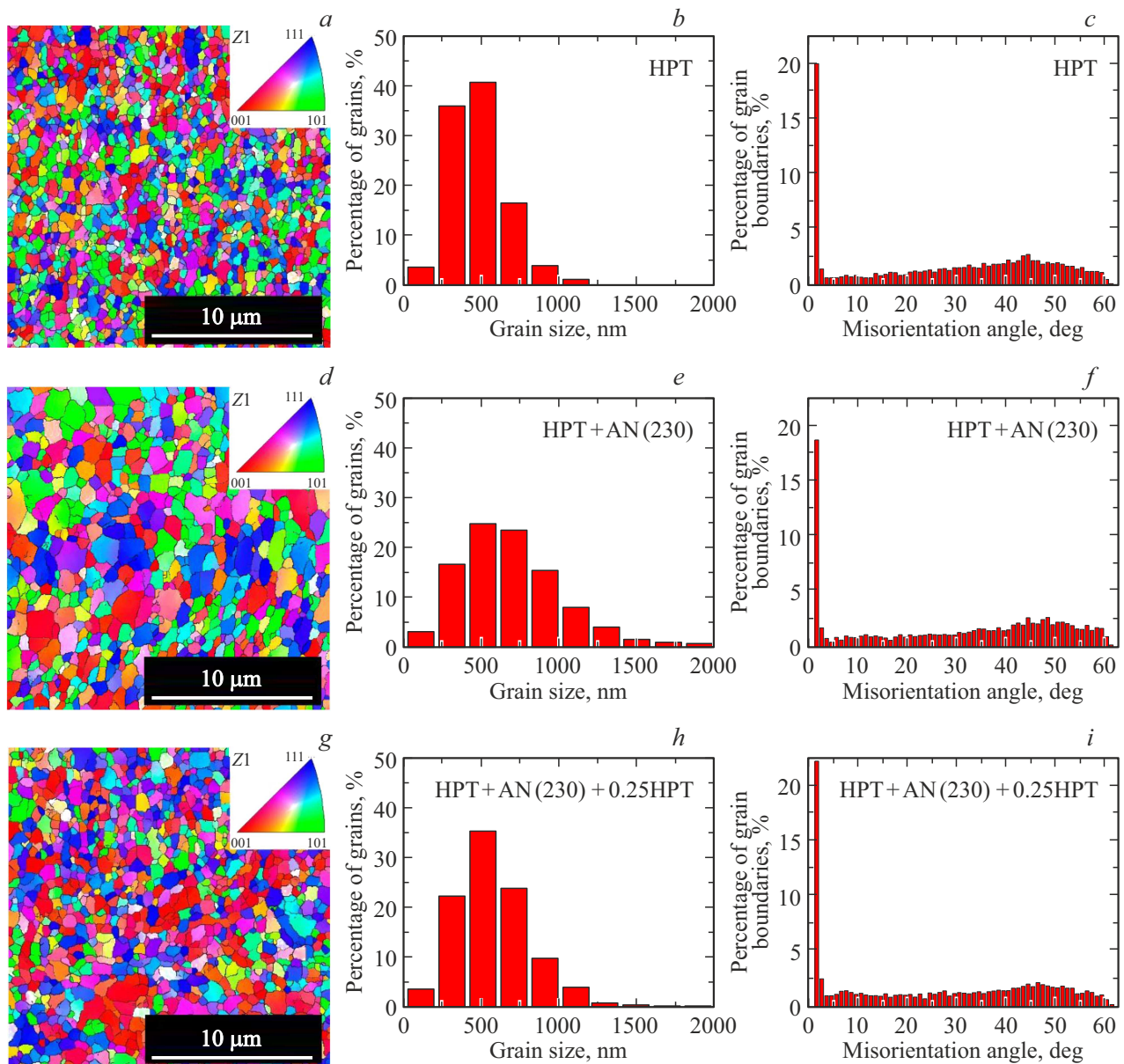


Figure 2. EBSD-maps (*a, d, g*), grain size distribution (*b, e, h*) and GB misorientation-angle distribution (*c, f, i*), obtained for UFG-Al-Mg-Zr in the following states: *a, b, c* — HPT; *d, e, f* — HPT + AN(230); *g, h, i* — HPT + AN(230) + 0.25HPT.

the unimodal nature of grain size distribution is maintained, however, there is a peak broadening towards large grain sizes (Figure 2, *e*). For this state (HPT + AN(230)) the EBSD map shows the presence of a large quantity of rather large grains with size of 900–2000 nm along with small grains. The fraction of grains with size $d_G \geq 900$ nm exceeds 30%. At the same time in the HPT state, and in the HPT + AN(150), HPT + AN(150) + 0.25HPT [14] states the fraction of grains with size of $d_G \geq 900$ nm does not exceed 5%.

In state HPT + AN(230) + 0.25HPT the average grain size decreases down to ~ 510 nm and becomes comparable to (differs slightly from) d_G in states HPT, HPT + AN(150) and HPT + AN(150) + 0.25HPT (Table 3). However, in

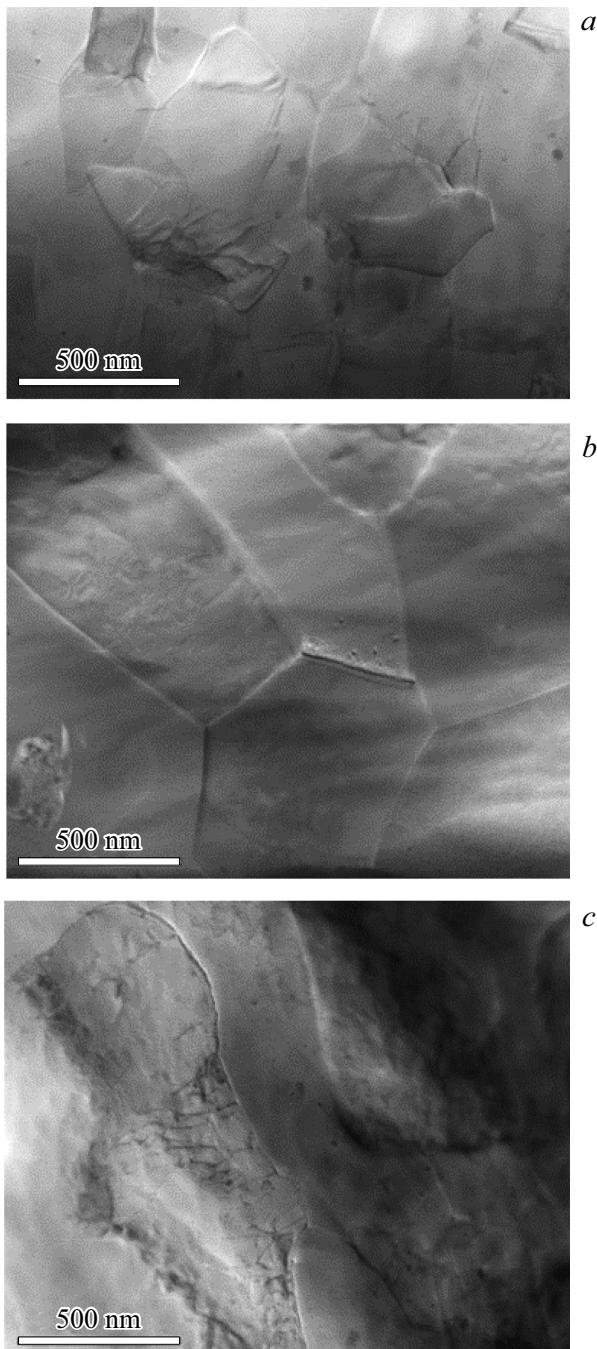
state HPT + AN(230) + 0.25HPT the fraction of grains with size $d_G \geq 900$ nm is maintained at the level of $\sim 20\%$ (Figure 2, *h*).

Figure 3 presents typical TEM-images obtained for UFG-alloy Al-0.95Mg-0.32Zr (wt.%) in different states.

In the HPT state there are practically no dislocations observed in the grains, except for some grains (Figure 3, *a*). GBs are distorted, blurred, which indicates their non-equilibrium state [25]. When annealed at 230 °C the GB structure relaxes and changes to a more equilibrium state, which is clearly seen on TEM: grain boundaries straighten, and the angle in the triple junctions becomes close to 120° (Figure 3, *b*). A somewhat developed dislocation structure in the body of the grains is still absent, but the number

Table 3. EBSD results obtained for UFG-Al-0.95Mg-0.32Zr (wt.%) in different states

State	d_G , nm	$f_{\geq 15}$, %	θ_{av} , deg	Reference
HPT	410 ± 60	70.6	28.8 ± 0.3	Pres. paper
HPT + AN(230)	690 ± 50	69.8	30.0 ± 0.3	
HPT + AN(230) + 0.25HPT	510 ± 30	62.1	26.1 ± 0.3	
HPT + AN(150)	470 ± 80	82.2	33.5 ± 0.3	[14]
HPT + AN(150) + 0.25HPT	480 ± 80	68.9	28.8 ± 0.3	

**Figure 3.** Typical TEM-images of the structure of UFG-alloy Al-0.95Mg-0.32Zr (wt.%) in different states: *a* — HPT, *b* — HPT + AN(230), *c* — HPT + AN(230) + 0.25HPT.

of single dislocations observed in the HPT state, decreased, which may be explained by the defect structure recovery processes. After AD by HPT method to $n = 0.25$ turns the GBs become blurred again, which indicates the increase in the degree of non-equilibrium in the grain-boundary structure. In some cases there are single dislocations and their clusters observed, being located directly near the GB and in the boundary areas (Figure 3, *c*).

In all the studied states we could see nano-precipitates of phase Al_3Zr with spherical shape. The belonging of these NPs to phase Al_3Zr is confirmed by EDXS measurements [10,14]. The character of Al_3Zr NP distribution in the volume is heterogeneous, and their number is small. As a result one may assume that most Zr atoms are in a solid solution. No noticeable change in the character of distribution and amount of precipitates Al_3Zr was found at both stages of DHT.

4. Discussion of results

Previously we demonstrated that in low-alloyed Al-Mg-Zr alloys, Mg is mostly in the solid solution with concentration that is slightly lower than the nominal one [10]. Excessive concentration of Mg is present in the form of segregations on GBs [14]. Indeed, the lattice parameter determined by the XRD method (Table 2) in the HPT state is $a \approx 4.0530 \text{ \AA}$, which by 0.0035 \AA exceeds the value of the parameter a in the pure Al ($a \approx 4.0745 \text{ \AA}$). Taking into account the fact that 1 at.% Mg increases the aluminum lattice parameter by $\sim 0.0046 \text{ \AA}$ [26], we find the concentration of Mg in the Al lattice equal approximately to 0.67 wt.%, which also indirectly indicates segregation of Mg on GB, since no Mg-containing precipitates were found, and Al atoms replacement with Zr atoms practically has no effect on the parameter value a [26]. These results match with some papers [14,27–32]. As it was demonstrated in papers [14,27,28], Mg atoms segregate easily at grain boundaries and triple junctions under severe plastic deformation by HPT method (deformation induced segregation). This is related to the fact that GBs act as stocks of vacancies formed in process of deformation by HPT [28,30]. According to [28], the interaction between the vacancies and Mg atoms leads to the movement of the latter to GBs and their segregation in the GBs.

After annealing at 230 °C the lattice parameter increased to $a = 4.0546 \text{ \AA}$, which corresponds to nominal concentration of magnesium $C_{\text{Mg}} \approx 0.97 \text{ wt.}\%$ in solid solution Al-Mg-Zr and now indicates that in the case of significant increase in grain size (Table 3), Mg segregations in boundaries of such grains may not be preserved. In state HPT + AN(230) + 0.25HPT $a = 4.0544 \text{ \AA}$, which corresponds to $C_{\text{Mg}} \approx 0.93 \text{ wt.}\%$. Such small reduction in the Mg concentration in a solid solution may indicate the formation of weak segregations of Mg atoms in GBs.

The yield stress in metals may be presented in the form of multiple strengthening contributions [33,34], such as grain boundary strengthening, determined by Hall–Petch ratio [35,36], solid solution strengthening (σ_{ss}), dispersion strengthening due to secondary phase nanoparticles, dislocation strengthening (σ_{dis}) and strengthening due to the lattice friction (Peierls–Nabarro stress, 10 MPa [37]).

As the studies of the microstructure (Tables 2 and 3) have shown, the specimens of UFG-alloy Al-0.95Mg-0.32Zr (wt.%) as a result of annealing at 230 °C, and also after the subsequent AD only the average grain size and the dislocation density change, and a small change in the Mg concentration in the solid solution arises (which can be concluded from the change in the parameter of the solid solution unit cell). Therefore, the change in the yield stress at both stages of DHT may be defined as the change of contributions from the grain-boundary and dislocation strengthening, and also strengthening from the solid solution

$$\Delta\sigma_{0.2} = \Delta\sigma_{\text{GB}} + \Delta\sigma_{\text{dis}} + \Delta\sigma_{\text{ss}}. \quad (3)$$

The contribution from grain boundary strengthening may be determined as [35,36]

$$\sigma_{\text{GB}} = Kd_{\text{av}}^{-1/2}, \quad (4)$$

where $K = 0.1 \text{ MPa}\cdot\text{m}^{1/2}$ is Hall-Petch coefficient for aluminum [38], d_{av} is average grain size.

Contribution from dislocation strengthening may be estimated as [39]

$$\sigma_{\text{dis}} = M\alpha GbL_{\text{dis}}^{1/2}, \quad (5)$$

where $M = 3.06$ is the Taylor factor [40], $\alpha = 0.33$ is the interdislocation interaction parameter [39], $G = 26 \text{ GPa}$ is the shear modulus, $b = 2.86 \text{ \AA}$ is the value of Burgers vector, L_{dis} is dislocation density.

Contribution from solid solution strengthening with Mg atoms [41]:

$$\sigma_{\text{ss}} = \sum k_i (C_i^{\text{ss}})^{2/3}, \quad (6)$$

where C_i^{ss} is concentration of i -nd alloying element in state of solid solution, $k_{\text{Mg}} = 29 \text{ MPa}(\text{wt.}\%)^{-2/3}$ [41], and $k_{\text{Zr}} = 9 \text{ MPa}(\text{wt.}\%)^{-2/3}$ [42].

The conducted estimates provide the theoretical value $\sim 95 \text{ MPa}$ for change of the yield stress $\Delta\sigma_{0.2}^{\text{th}}$ after annealing at 230 °C. And the contribution $\Delta\sigma_{\text{ss}}$ is low ($\sim 6.5 \text{ MPa}$; note that the estimate $\Delta\sigma_{\text{ss}}$ took into

account the change of only Mg concentration in the solid solution, believing that Zr concentration is not changing, since no significant difference was found in the size, concentration and distribution of the secondary phase Al_3Zr after annealing at 230 °C and subsequent AD). At the same time the experimentally derived difference in the strengthening for HPT and HPT + AN(230) states is $\Delta\sigma_{0.2}^{\text{exp}} \approx 230 \text{ MPa}$ (the values of $\sigma_{0.2}$ in Table 1). The difference between $\Delta\sigma_{0.2}^{\text{th}}$ and $\Delta\sigma_{0.2}^{\text{exp}}$, making $\sim 135 \text{ MPa}$, is related, most probably, to additional strengthening due to grain boundary segregations of Mg in the HPT state and unpinnig of grain boundaries from these segregations as a result of significant grain growth during annealing at higher $T_{\text{AN}} = 230 \text{ }^\circ\text{C}$. As it was shown previously for alloy Al-0.53Mg-0.27Zr (wt.%), structuring by HPT method under similar conditions causes Mg segregation at GBs, which provide comparative value of additional strengthening $\sim 150 \text{ MPa}$ [10]. Estimate of the yield stress change in case of annealing of UFG alloy Al-0.95Mg-0.32Zr (wt.%) at 150 °C provides the value $\Delta\sigma_{0.2}^{\text{th}} \approx 75 \text{ MPa}$, comparable to the experimentally observed value $\Delta\sigma_{0.2}^{\text{exp}} \sim 70 \text{ MPa}$ (Table 1). When annealed at $T_{\text{AN}} = 150 \text{ }^\circ\text{C}$ average grain size varies slightly (Table 3), which explains the preservation of the additional strengthening due to segregations in GBs at such low temperature annealing. Therefore, annealing at 230 °C differs in principle from annealing at lower temperature 150 °C: in the first case most GBs are unpinned from Mg segregations on them, while in the second case the GB pinning by Mg segregations is mostly preserved.

As a result of AD to $n = 0.25$ turns after annealing 230 °C (state HPT + AN(230) + 0.25HPT) additional strengthening occurs by $\Delta\sigma_{0.2}^{\text{exp}} = 125 \text{ MPa}$ (Table 1, Figure 1). Taking into account the change of the grain size, dislocation density and minor decrease of Mg concentration in the solid solution (according to the lattice parameter change), additional strengthening after AD was $\Delta\sigma_{0.2}^{\text{th}} = 67 \text{ MPa}$, which is $\sim 60 \text{ MPa}$ lower than the experimental value $\Delta\sigma_{0.2}^{\text{exp}} = 125 \text{ MPa}$. This additional strengthening $\sim 60 \text{ MPa}$ is most probably related to formation of new segregations in GB (less strong and/or more unevenly distributed in the grain-boundary structure compared to the original state HPT). Additional HPT deformation to 0.25 turns after annealing at 230 °C (state HPT + AN(230) + 0.25HPT) causes decrease of the average grain size from 690 to 510 nm, i.e. additional refinement of the structure occurs, which is accompanied with formation of new GBs and increase of total non-equilibrium of the GB structure by addition of external dislocations into the GB structure in the process of AD. In paper [43] for alloy Al-3%Mg and paper [44] for alloy Al-Cu-Mg it was shown that at very early stages of HPT ($n = 0.25$ turns), deformation-induced segregation of Mg atoms at GB takes place. Possibly, as a result of AD to 0.25 turns after annealing at 230 °C the deformation-induced segregation of Mg atoms to the GBs free of segregation also takes place, which provides additional strengthening. This, in its turn, causes a contribution from the segregation strengthening

and explains considerable increase of strength in the state HPT + AN(230) + 0.25HPT compared to the state after annealing.

Higher ductility in the state HPT + AN(230) + 0.25HPT compared to the state HPT + AN(150) + 0.25HPT is possibly due to the presence of the considerable amount of ($\sim 20\%$) quite large grains ($d_G = 900\text{--}2000\text{ nm}$) in the ultrafine-grained structure in the first case, where plastic deformation may develop more actively, which helps to implement high ductility of UFG-alloy Al-0.95Mg-0.32Zr (wt.%) with preservation of its high strength. The obtained result indicates new capabilities of implementing the higher ductility in conductor UFG-alloys based on the Al-Mg-Zr system.

5. Conclusion

The paper for the first time studied the effect of DHT consisting of annealing at elevated temperature 230°C for 1 h and additional deformation by HPT method to 0.25 turns, on microstructure, and resulting properties of UFG-alloy Al-0.95Mg-0.32Zr (wt.%), structured by HPT method to $n = 10$ turns. The following results were obtained:

1. When annealed at 230°C and subsequently additionally deformed by HPT to 0.25 turns (state HPT + AN(230) + 0.25HPT), UFG-alloy Al-0.95Mg-0.32Zr (wt.%) behaves as a CG-material at both stages: annealing promotes softening and increases ductility, and additional deformation, on the contrary, increases strength and reduces ductility. As a result of using such DHT (state HPT + AN(230) + 0.25HPT)), ductility was increased substantially to $\delta \approx 10\%$ ($\delta_1 > 2\%$) with preservation of high level of strength (yield stress $\sim 340\text{ MPa}$, ultimate tensile strength $\sim 390\text{ MPa}$) and electrical conductivity ($\sim 48.4\%$ IACS). The produced combination of properties is only slightly inferior in strength, and by ductility it exceeds the achieved characteristics as a result of using such DHT with annealing temperature 150°C (state HPT + AN(150) + 0.25HPT).

2. The conducted analysis of the microstructure-properties ratio shows that increased ductility as a result of DHT with the higher temperature of annealing 230°C is due to the introduction of additional dislocation density into grain boundaries and near-boundary areas relaxed by annealing, decrease of Mg segregation at GB, and introduction of a fraction ($\sim 20\%$) of larger grains in the GB distribution on size. Preservation of strength at level $\sim 75\%$ of strength in the initial UFG-state is provided by preservation of small average grain size ($\sim 510\text{ nm}$) and, most probably, formation of new weaker and/or more heterogeneous segregations of Mg at GB. Peculiarities of such segregations formation require detailed microscopic study with involvement of methods of atom probe tomography in virtue of low concentration of alloying elements in the studied alloys.

Acknowledgments

XDA, EBSD and TEM/STEM studies were carried out using the equipment and software of the Center of Joint Use „Materials Science and Diagnostics in Advanced Technologies“ (Ioffe Institute, St. Petersburg, Russia).

Conflict of interest

The authors declare that they have no conflict of interest.

References

- [1] M.Yu. Murashkin, N.A. Enikeev, X. Sauvage. *Mater. Trans.* **64**, 8, 1833 (2023).
- [2] R.Z. Valiev, M.Y. Murashkin, I. Sabirov. *Scripta Materialia* **76**, 13 (2014).
- [3] T. Knych, M. Piwowska, P. Uliasz. *Arch. Met. Mater.* **56**, 685 (2011).
- [4] D.I. Bely. *Kabeli i provoda* **332**, 8 (2012). (in Russian).
- [5] ASTM B941-16, Standard Specification for Heat Resistant Aluminum Zirconium Alloy Wire for Electrical Purposes. ASTM International: West Conshohocken, PA (2016).
- [6] P.H.L. Souza, C.A. Silva de Oliveira, J.M. do Vale Quaresma. *Mater. Res. Technol.* **7**, 1, 66 (2018).
- [7] K.E. Knipling, D.C. Dunand, D.N. Seidman. *Int. J. Mater. Res.* **97**, 3, 246 (2022).
- [8] Y. Iwahashi, Z. Horita, M. Nemoto, T.G. Langdon. *Metall. Metal. Trans. A* **29**, 10, 2503 (1998).
- [9] J. Gubicza, N.Q. Chinh, Z. Horita, T.G. Langdon. *Mater. Sci. Eng. A* **387–389**, 55 (2004).
- [10] T.S. Orlova, T.A. Latynina, M.Y. Murashkin, F. Chabanais, L. Rigutti, W. Lefebvre. *J. Alloys Compd.* **859**, 157775 (2021).
- [11] M.Y. Murashkin, A.E. Medvedev, V.U. Kazykhanov, G.I. Raab, I.A. Ovid'ko, R.Z. Valiev. *Rev. Adv. Mater. Sci.* **47**, 1/2, 16 (2016).
- [12] T.S. Orlova, A.M. Mavlyutov, D.I. Sadykov, N.A. Enikeev, M.Yu. Murashkin. *Metals* **13**, 9, 1570 (2023).
- [13] A.M. Mavlyutov, T.S. Orlova, M.Y. Murashkin, N.A. Enikeev, D.A. Kirilenko. *Fizicheskaya Mezomekhanika*, **28**, 1, 5 (2025). (in Russian).
- [14] D.I. Sadykov, M.Yu. Murashkin, D.A. Kirilenko, A.A. Levin, A.I. Likhachev, T.S. Orlova. *FTT* **66**, 6, 933 (2024). (in Russian).
- [15] DIFFRAC.EVA. Version 5.1.0.5. Bruker AXS, Karlsruhe, Germany (2019).
- [16] Powder Diffraction File-2, International Centre for Diffraction Data (ICDD). Newton Square, PA, USA (2014).
- [17] C. Maunders, J. Etheridge, N. Wright, H.J. Whitfield. *Acta Crystallographica B* **61**, Part 2, 154 (2005).
- [18] A.A. Levin. Preprint (2022). <https://doi.org/10.13140/RG.2.2.15922.89280>
- [19] B. Terlan, A.A. Levin, F. Börrnert, F. Simon, M. Oschatz, M. Schmidt, R. Cardoso-Gil, T. Lorenz, I.A. Baburin, J.-O. Joswig, A. Eychmüller. *Chem. Mat.* **27**, 14, 5106 (2015).
- [20] B. Terlan, A.A. Levin, F. Börrnert, J. Zeisner, V. Kataev, M. Schmidt, A. Eychmüller. *Eur. J. Inorg. Chem.* **2016**, 21, 3460 (2016).
- [21] G.K. Williamson, R.E. Smallman. *Philos. Mag.* **1**, 1, 34 (1956).
- [22] K. Edalati, N. Enikeev. *Mater.* **17**, 24, 6189 (2024).

- [23] J.P. Hirth, J. Lothe. Theory of Dislocations. McGraw-Hill, N.Y. (1968). 780 p.
- [24] T.S. Orlova, D.I. Sadykov, D.V. Danilov, M.Y. Murashkin. *J. Alloys Compd.* **931**, 167540 (2023).
- [25] M. Zha, H. Zhang, H. Jia, Y. Gao, S. Jin, G. Sha, R. Bjørge, R.H. Mathiesen, H.J. Roven, H. Wang, Y. Li. *Int. J. Plast.* **146**, 103108 (2021).
- [26] J.E. Hatch. Aluminum: Properties and Physical Metallurgy, 1st ed. ASM International, Metals Park, OH (1984).
- [27] Y. Liu, M. Liu, X. Chen, Y. Cao, H.J. Roven, M.Yu. Murashkin, R.Z. Valiev, H. Zhou. *Scripta Materialia* **159**, 137 (2019).
- [28] X. Sauvage, N. Enikeev, R. Valiev, Y. Nasedkina, M. Murashkin. *Acta Materialia* **72**, 125 (2014).
- [29] M.P. Liu, H.J. Roven, M.Yu. Murashkin, R.Z. Valiev, A. Kilmametov, Z. Zhang, Y. Yu. *J. Mater. Sci.* **48**, 13, 4681 (2013).
- [30] X. Sauvage, A. Ganeev, Yu. Ivanisenko, N. Enikeev, M. Murashkin, R. Valiev. *Adv. Eng. Mater.* **14**, 11, 968 (2012).
- [31] I. Sabirov, M.Yu. Murashkin, R.Z. Valiev. *Mater. Sci. Eng. A* **560**, 1 (2013).
- [32] Y. Zhang, S. Jin, P. Trimby, X. Liao, M.Y. Murashkin, R.Z. Valiev, G. Sha. *Mater. Sci. Eng. A* **752**, 223–232 (2019).
- [33] N. Kamikawa, X. Huang, N. Tsuji, N. Hansen. *Acta Materialia* **57**, 14, 4198 (2009).
- [34] H. Asgharzadeh, A. Simchi, H.S. Kim. *Mater. Sci. Eng. A* **528**, 12, 3981 (2011).
- [35] E.O. Hall. *Proceed. Phys. Soc. B.* **64**, 9, 747 (1951).
- [36] N.J. Petch. *J. Iron Steel Inst.* **174**, 25 (1953).
- [37] G.E. Totten, D.S. MacKenzie. *Handbook of Aluminium*. Marcel Dekker, NY (2003). 1310 p.
- [38] M. Zha, H.-M. Zhang, X.-T. Meng, H.-L. Jia, S.-B. Jin, G. Sha, H.-Y. Wang, Y.-J. Li, H.J. Roven. *J. Mater. Sci. Tech.* **89**, 141 (2021).
- [39] F.R.N. Nabarro, Z.S. Basinski, D.B. Holt. *Adv. Phys.* **13**, 50, 193 (1964).
- [40] N. Hansen, X. Huang. *Acta Materialia* **46**, 5, 1827 (1998).
- [41] O.R. Myhr, Ø. Grong, S.J. Andersen. *Acta Materialia* **49**, 1, 65 (2001).
- [42] K.E. Knipling, D.C. Dunand, D.N. Seidman. *Acta Materialia* **56**, 1, 114 (2008).
- [43] H.-J. Lee, J.-K. Han, S. Janakiraman, B. Ahn, M. Kawasaki, T.G. Langdon. *J. Alloys Compd.* **686**, 998 (2016).
- [44] Y. Chen, N. Gao, G. Sha, S.P. Ringer, M.J. Starink. *Mater. Sci. Eng. A* **627**, 10 (2015).

Translated by M.Verenikina